Understanding the K^*/K ratio in heavy ion collisions

C. Le Roux [a], F.S. Navarra [a,*], L.M. Abreu [b]

[a] *Instituto de Física, Universidade de São Paulo, Rua do Matão, 1371, CEP 05508-090, São Paulo, SP, Brazil*
[b] *Instituto de Física, Universidade Federal da Bahia, Campus Universitário de Ondina, 40170-115, Bahia, Brazil*

ARTICLE INFO

ABSTRACT

We study the K^* meson dissociation in heavy ion collisions during the hadron gas phase. We use the production and absorption cross sections of the K^* and K mesons in a hadron gas, which were calculated in a previous work. We compute the time evolution of the K^* abundance and the K^*/K ratio during the hadron gas phase. Assuming a Bjorken type cooling and using an empirical relation between the freeze-out temperature and the central multiplicity density, we are able to write K^*/K as a function of $(dN/d\eta(\eta=0))$. The obtained function is in very good agreement with recent experimental data.

© 2021 The Author(s). Published by Elsevier B.V. This is an open access article under the CC BY license (http://creativecommons.org/licenses/by/4.0/). Funded by SCOAP³.

1. Introduction

In recent heavy ion collision experiments nuclei are accelerated towards each other with energies of the order of GeV or TeV. These extremely high energies allow for the production of a deconfined phase of quarks and gluons. This phase where the fundamental particles are able to travel freely is known as the quark gluon plasma (QGP) [1,2]. It exists for a short time and as the system expands and cools down, quarks, antiquarks and gluons recombine to form hadrons. This phase transition back to the hadron phase is also called hadronization. The abundances of particles formed during the hadronization depend on the temperature and on the baryon chemical potential. After hadronization the system becomes a hot hadron gas in which inelastic reactions occur, changing the relative abundance of the hadrons. The system further expands and cools down until the point when all interactions cease. This is known as kinetic or thermal freeze-out. The final yield of hadrons in a collision is influenced not only by their production rate at the quark-hadron transition point but also by the interactions that they undergo after hadronization, which might increase or decrease their abundances. At the thermal freeze-out, particle abundances are frozen and the hadrons flow freely to the detectors.

The K^* meson is a resonance and may change its abundance also by the strong decay $K^* \to K\pi$. This meson has a lifetime of 4 fm/c, smaller than the duration of the hadron gas phase, which is believed to be of the order of 10 fm/c. When the decay happens in the hadronic medium, the daughter particles (K and π) interact further with other particles in the environment, changing their energy and momentum, and even if they can be measured at the end of the heavy ion collision, the invariant mass of the pair is no longer equal to the K^* mass. The K^* which is no longer reconstructed is lost and we would observe a reduction in the final yield of this resonance, which would then be attributed to the existence of the hadron gas phase. This means that the existence of the hadron gas phase could be tested by the study of the abundances of such particles. This idea has been discussed in several publications [3–8].

From the experimental point of view, the abundance of the K^* meson can be studied through the yield ratio K^*/K. Experiments have measured it to be 0.33 ± 0.01 in Au+Au collisions at $\sqrt{s_{NN}} = 130$ GeV, 0.23 ± 0.05 in Au+Au collisions at $\sqrt{s_{NN}} = 200$ GeV at RHIC [9,10], 0.19 ± 0.05 at $\sqrt{s_{NN}} = 2.76$ TeV in Pb+Pb collisions at the LHC [11,12] and very recently [13] it was found to be 0.2 ± 0.01 in Pb+Pb at $\sqrt{s_{NN}} = 5.02$ TeV in collisions at the LHC. Model calculations suggest that the lifetime of the hadron gas phase grows with the mass of the colliding nuclei, with centrality and with the collision energy. We can see that the ratio K^*/K decreases as the collision energy and/or system size increases, giving support to the conjecture made in the previous paragraph. However, in order to reach a firm conclusion a comprehensive quantitative calculation must be done.

* Corresponding author.
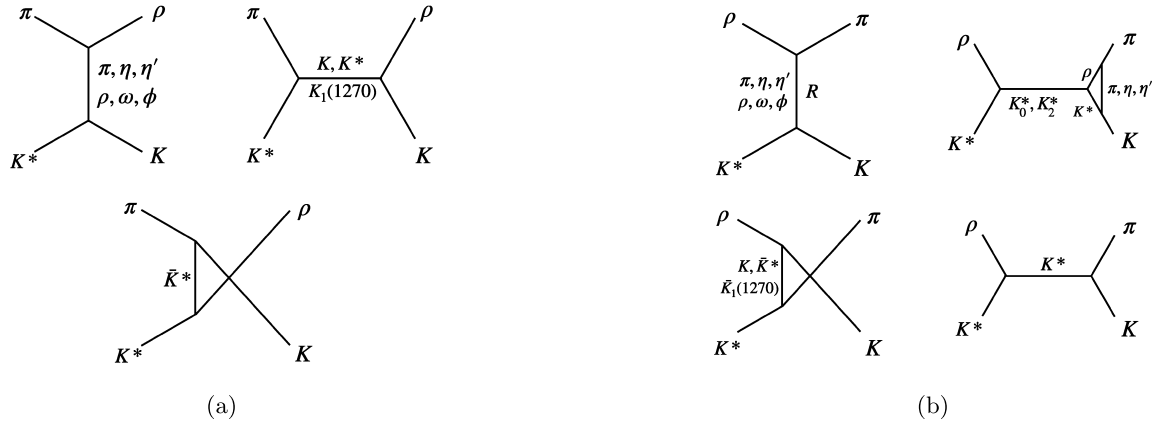 *E-mail address:* navarra@if.usp.br (F.S. Navarra).

Fig. 1. Diagrams for the relevant processes considered in the calculation of the cross sections in Ref. [17]. a) $K^*\pi \to \rho K$ reactions. R represents the resonances $h_1(1170)$, $h_1(1380)$, $f_1(1285)$, $a_1(1260)$ and $b_1(1235)$. b) $K^*\rho \to K\pi$ reactions.

In the hadron gas formed in heavy ion collisions, the temperatures range from $\simeq 175$ MeV, where hadronization takes place, to $\simeq 100$ MeV, where kinetic freeze-out takes place. The temperature defines the order of magnitude of the hadron momenta in the gas and also the energy with which hadrons collide in the medium. The energies of a few hundred MeV's are too high to allow the use of chiral perturbation theory and are too low to allow the use of perturbative QCD. One has to resort to models involving mesons and baryons. In principle baryons could be efficient in absorbing K^*'s. Although the coupling constants $BB'K^{(*)}$ (baryon-baryon-strange meson) are relatively small [14], it has been shown in [15] that the interaction cross sections are significant and the K^*N total cross section can be as large as 20 mb. On the other hand, the particles which emerge from the hadron gas have low or moderate rapidities and in this rapidity region there are no remnant baryons from the projectile or from the target. There are only newly created baryons, which are relatively rare. Therefore, here we follow [16] and neglect K^* interactions with baryons.

In Ref. [16] the authors computed the cross sections of several types of interactions suffered by K^* and K mesons in the hadron gas and showed that, due to these interactions and to the strong decay, the final yield ratio K^*/K measured in central Au+Au collision at $\sqrt{s_{NN}} = 200$ GeV decreases by 37% during the hadron gas phase, resulting in a final ratio comparable to STAR measurements. In [16], the change in the abundances of the K^* and K mesons was computed by solving a system of differential rate equations which use as input the cross sections for different interactions involving the K^* and K mesons with each other and with the light mesons ρ and π. The authors found that the leading processes contributing to the abundance dynamics are: $K^*\pi \to K\rho$, $K^*\rho \to K\pi$ and $K^* \to K\pi$, as well as the inverse ones.

In [16] some interaction mechanisms that might be relevant were not included in the calculations. In a subsequent work [17] the cross sections for production and annihilation of K^* and K mesons were recalculated with the inclusion of new reaction mechanisms. The relevant Feynman diagrams for the $K^*\pi \to \rho K$ and $K^*\rho \to K\pi$ reactions are shown in Fig. 1.

The most important (but not the only ones) changes made in [17] are:

I) Inclusion of anomalous parity vector-vector-pseudoscalar (VVP) interactions.
II) Inclusion of the exchange of axial resonances $K_1(1270)$, $h_1(1170)$, $h_1(1380)$, $f_1(1285)$, $a_1(1260)$ and $b_1(1235)$ in the s and t channels.

Modification I) introduces new vertices, modifies several Feynman diagrams and changes the amplitudes of all processes discussed previously in [16]. In Refs. [18–20], it was shown that interaction terms with anomalous parity couplings have a strong impact on the corresponding cross sections. The relevance of such anomalous terms in the determination of the abundance of $X(3872)$ in heavy ion collisions was computed in Ref. [21]. In [17] these interaction terms were found to be relevant also in the calculation of K^* absorption processes. Modification II) introduces several new diagrams. The presence of the resonance $K_1(1270)$, for example, had been found to be important [22] in describing the invariant mass distribution of the process $K^-p \to K^-\pi^+\pi^-p$ at $\sqrt{s_{NN}} = 63$ GeV measured by the WA3 collaboration at CERN [23]. In [17] it was seen that the diagram with $K_1(1270)$ in the s-channel is the most important contribution to the absorption process $\pi K^* \to \omega K$ and also to the production process $\rho K \to \pi K^*$.

The results in Ref. [17] show that the new mechanisms are rather significant, changing the cross sections up to one or two orders of magnitude in some cases, suggesting that these new cross sections would result in a very different dynamics for the abundances of K^* and K mesons. A comparison between the results obtained in Refs. [16] and in [17] is presented in Fig. 2, where we show the thermally averaged cross sections (see below) of the main processes of absorption and regeneration of K^*. From the figures we see that the cross sections found in [17] are much larger than those found in [16], both for absorption and for regeneration of K^*.

In this work we use the improved cross sections of [17] and solve the differential rate equations proposed in Ref. [16], obtaining the K^*/K ratio as a function of the proper time. We use a Bjorken type cooling to connect the proper time and the temperature. The evolution stops at the freeze-out temperature T_f. Finally, we use the empirical relation between T_f and the central multiplicity density found in [24], to obtain a direct relation between the K^*/K ratio and $dN/d\eta(\eta = 0)$. The obtained relation is in very good agreement with experimental data. In the next section we briefly describe the formalism and in the following section we present our results and compare them with experimental data.

2. Formalism

2.1. Thermal cross sections

In [16] the interactions of K and K^* with light non-strange mesons were described by effective Lagrangians of the type $\mathcal{L}_{PPV}$ and $\mathcal{L}_{VVV}$, where P and V are pseudoscalar and vector mesons, respectively. The Lagrangians were obtained from free pseudoscalar and vector meson Lagrangians by introducing the minimal substitution. In [17], in addition to these Lagrangians, the Lagrangian $\mathcal{L}_{VVP}$ was included, representing the so called "anomalous parity" interactions. From the Lagrangians it is straightforward to evaluate the amplitudes of K^* absorption by pions, kaons, ρ's and by K^*'s. In order to take the finite size of the hadrons into consideration when evaluating amplitudes, one uses form factors at each interaction vertex. These form factors contain a cut-off parameter. In [16] the authors took a value taken from previous phenomenological analyses [25]. With the amplitudes it is easy to compute the cross sections of the corresponding processes. With the same Lagrangians one can calculate all the interaction cross sections of kaons. Moreover, with the use of detailed balance one can calculate the inverse processes, i.e. one can compute the $K^* + \pi \to K + \rho$ and $K + \rho \to K^* + \pi$ cross sections. Finally, one has to consider the processes $K + \pi \to K^*$ and $K^* \to K + \pi$. The authors of [16] also found that the cross section for the formation of the K^* meson from pions and K mesons is not small at all, compared to cross sections for other processes.

All the reactions mentioned above happen within a hadron gas at temperatures ranging from 100 to 200 MeV. These temperatures determine the collision energies. Moreover the densities of the colliding particles are determined by the temperature. Therefore, in this context, the most relevant dynamical quantity is the thermally averaged cross section. For a process $a + b \to c + d$ it is defined as:

$$\langle \sigma_{ab \to cd} v_{ab} \rangle = \frac{1}{1 + \delta_{ab}} \frac{\int d^3 \vec{p}_a d^3 \vec{p}_b f_a(\vec{p}_a) f_b(\vec{p}_b) \sigma_{ab \to cd} v_{ab}}{\int d^3 \vec{p}_a d^3 \vec{p}_b f_a(\vec{p}_a) f_b(\vec{p}_b)}, \tag{1}$$

where v_{ab} is the relative velocity between the initial particles

$$v_{ab} = \sqrt{(p_a \cdot p_b)^2 - m_a^2 m_b^2} / (E_a E_b)$$

and $f_i(\vec{p}_i)$ is the thermal momentum distribution of particle i, which is given by a Bose-Einstein distribution:

$$f_i(\vec{p}_i) = \frac{1}{e^{\sqrt{\vec{p}_i^2 + m_i^2}/T} - 1}.$$

The production and absorption rates of K^* or K obviously depend on the densities of particles in the hadron gas at proper time τ which are given by

$$n_i(\tau) = \frac{g_i}{2\pi^2} \int_0^\infty \frac{p^2 dp}{e^{\sqrt{p_i^2 + m_i^2}/T(\tau)} - 1} \simeq \frac{g_i}{2\pi^2} m_i^2 T(\tau) K_2 \left(\frac{m_i}{T(\tau)} \right), \tag{2}$$

where g_i is the degeneracy factor of meson i and m_i its mass. $K_2(\tau)$ is the modified Bessel function of the second kind and $T(\tau)$ is the temperature. The total number of particles of species i, $N_i(\tau)$, is obtained by multiplying the density given by (2) by the system volume $V(\tau)$. At last, the thermally averaged decay width of K^* was computed using the following expression introduced in Ref. [16]:

$$\langle \Gamma_{K^*} \rangle = \Gamma_{K^*}(m_{K^*}) \frac{K_1 \left(\frac{m_{K^*}}{T(\tau)} \right)}{K_2 \left(\frac{m_{K^*}}{T(\tau)} \right)}, \tag{3}$$

where K_1 and K_2 are the modified Bessel functions of the first and second kind, $T(\tau)$ is the temperature as a function of proper time τ, m_{K^*} is the mass of K^* and Γ_{K^*}, its decay width, which was computed as:

$$\Gamma_{K^*}(\sqrt{s}) = \frac{g_{\pi K K^*}^2}{2\pi s} p_{cm}^3(\sqrt{s}), \tag{4}$$

with $g_{\pi K K^*}$ being the coupling constant, p_{cm} the momentum at the center of mass frame and s the Mandelstam variable.

For our purposes it is not necessary to recalculate all the thermally averaged cross sections, $\langle \sigma_{ab \to cd} v_{ab} \rangle$, which are smooth functions of the temperature. It is enough to parametrize the results obtained in Refs. [16] and [17] by the polynomial functions which are shown in the Appendix. The resulting parametrizations are shown in Fig. 2.

In Fig. 2 we can compare the results obtained in [16] with those obtained in [17]. The inclusion of modifications I and II increased the cross sections typically by one order of magnitude. In both approaches the absorption of K^* is stronger than its production. However, with the formalism considered in [17], at higher temperatures we observe the dominance of the processes of creation of K^*. So, when the hadron gas starts its expansion at high temperatures, we expect to see first the growth of the K^* multiplicity which is later followed by its reduction. In contrast, with the formalism of [16] we only see a monotonic reduction of the K^* multiplicity.

2.2. Evolution equations

With the ingredients presented in the previous subsection, it is possible to write rate equations, which describe the time evolution of the K^* and K multiplicities, incorporating the gain and loss terms due to production and absorption respectively. These equations are:

(a)   (b)
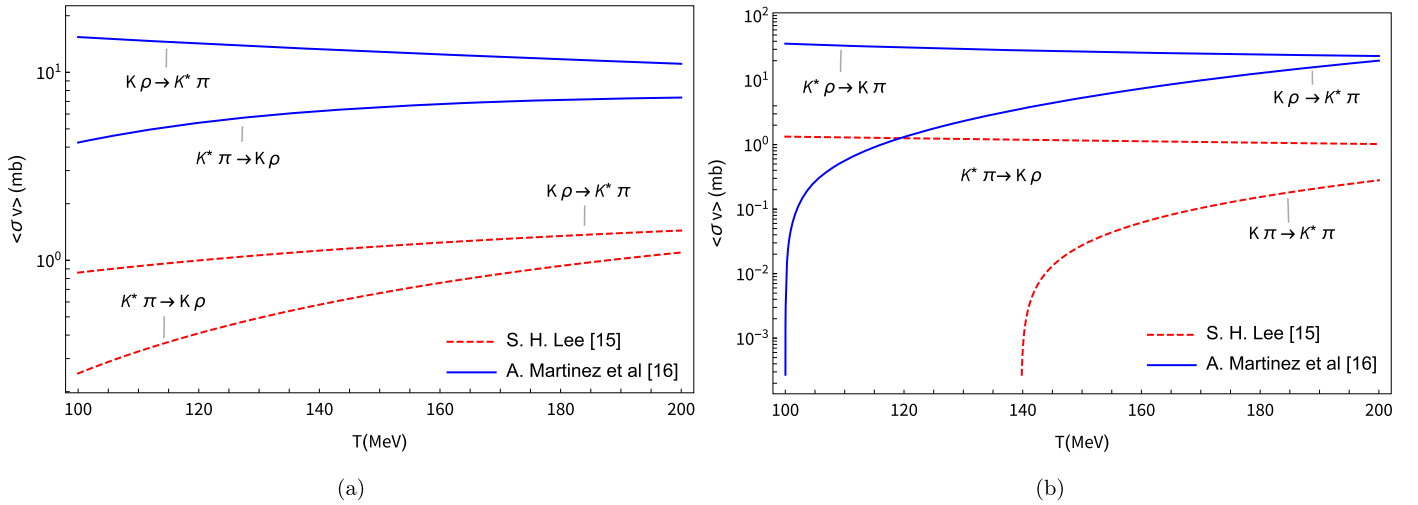
Fig. 2. Comparison between the cross sections obtained in Ref. [16] and those obtained in Ref. [17]. The lines are obtained with Eq. (16) which is a parametrization of the results obtained in the mentioned papers. a) $K^*\pi \to \rho K$ reactions. b) $K^*\rho \to K\pi$ reactions.

$$\frac{dN_{K^*}}{d\tau} = \langle \sigma_{K\rho \to K^*\pi} v_{K\rho} \rangle n_\rho(\tau) N_K(\tau) - \langle \sigma_{K^*\pi \to K\rho} v_{K^*\pi} \rangle n_\pi(\tau) N_{K^*}(\tau) + \langle \sigma_{K\pi \to K^*\rho} v_{K\pi} \rangle n_\pi(\tau) N_K(\tau)$$

$$- \langle \sigma_{K^*\rho \to K\pi} v_{K^*\rho} \rangle n_\rho(\tau) N_{K^*}(\tau) + \langle \sigma_{\pi\rho \to K^*\bar{K}} v_{\pi\rho} \rangle n_\pi(\tau) N_\rho(\tau) - \langle \sigma_{K^*\bar{K} \to \rho\pi} v_{K^*\bar{K}} \rangle n_{\bar{K}}(\tau) N_{K^*}(\tau)$$

$$+ \langle \sigma_{\pi\pi \to K^*\bar{K}^*} v_{\pi\pi} \rangle n_\pi(\tau) N_\pi(\tau) - \langle \sigma_{K^*\bar{K}^* \to \pi\pi} v_{K^*\bar{K}^*} \rangle n_{\bar{K}^*}(\tau) N_{K^*}(\tau) + \langle \sigma_{\rho\rho \to K^*\bar{K}^*} v_{\rho\rho} \rangle n_\rho(\tau) N_\rho(\tau)$$

$$- \langle \sigma_{K^*\bar{K}^* \to \rho\rho} v_{K^*\bar{K}^*} \rangle n_{\bar{K}^*}(\tau) N_{K^*}(\tau) + \langle \sigma_{K\pi \to K^*} v_{K\pi} \rangle n_\pi(\tau) N_K(\tau) - \langle \Gamma_{K^*} \rangle N_{K^*}(\tau),$$

$$\frac{dN_K}{d\tau} = \langle \sigma_{\pi\pi \to K\bar{K}} v_{\pi\pi} \rangle n_\pi(\tau) N_\pi(\tau) - \langle \sigma_{K\bar{K} \to \pi\pi} v_{K\bar{K}} \rangle n_{\bar{K}}(\tau) N_K(\tau) + \langle \sigma_{\rho\rho \to K\bar{K}} v_{\rho\rho} \rangle n_\rho(\tau) N_\rho(\tau)$$

$$- \langle \sigma_{K\bar{K} \to \rho\rho} v_{K\bar{K}} \rangle n_{\bar{K}}(\tau) N_K(\tau) + \langle \sigma_{K^*\pi \to K\rho} v_{K^*\pi} \rangle n_\pi(\tau) N_{K^*}(\tau) - \langle \sigma_{K\rho \to K^*\pi} v_{K\rho} \rangle n_\rho(\tau) N_K(\tau)$$

$$+ \langle \sigma_{K^*\rho \to K\pi} v_{K^*\rho} \rangle n_\rho(\tau) N_{K^*}(\tau) - \langle \sigma_{K\pi \to K^*\rho} v_{K\pi} \rangle n_\pi(\tau) N_K(\tau) + \langle \sigma_{\pi\rho \to K^*\bar{K}} v_{\pi\rho} \rangle n_\pi(\tau) N_\rho(\tau)$$

$$- \langle \sigma_{K^*\bar{K} \to \rho\pi} v_{K^*\bar{K}} \rangle n_{\bar{K}}(\tau) N_{K^*}(\tau) + \langle \Gamma_{K^*} \rangle N_{K^*}(\tau) - \langle \sigma_{K\pi \to K^*} v_{K\pi} \rangle n_\pi(\tau) N_K(\tau). \tag{5}$$

The above equations include all relevant creation and annihilation reactions. However, as showed in Refs. [16] and [17], some of them have very small thermally averaged cross sections and can be safely neglected. The really important interactions of the K^* meson according to both references are the following:

$$K^*\rho \to K\pi,$$
$$K^*\pi \to K\rho,$$
$$K^* \to K\pi, \tag{6}$$

as well as the respective inverse processes. This should not be surprising since π's are the most abundant particles in a hadron gas and ρ's are vector particles and, as discussed above, have a large interaction cross section with other vector particles. Restricting ourselves to the processes above, the system of differential equations Eq. (5) can be written as:

$$\frac{dN_{K^*}(\tau)}{d\tau} = \gamma_K N_K(\tau) - \gamma_{K^*} N_{K^*}(\tau),$$
$$\frac{dN_K(\tau)}{d\tau} = -\gamma_K N_K(\tau) + \gamma_{K^*} N_{K^*}(\tau), \tag{7}$$

where N_K and N_{K^*} are the abundances of K and K^* mesons respectively. They are functions of the proper time τ. The factors γ_K and γ_{K^*} depend on the interaction cross sections and the light meson densities in the following way:

$$\gamma_K = \langle \sigma_{K\pi \to K^*\rho} v_{K\pi} \rangle n_\pi + \langle \sigma_{K\rho \to K^*\pi} v_{K\rho} \rangle n_\rho + \langle \sigma_{K\pi \to K^*} v_{K\pi} \rangle n_\pi,$$
$$\gamma_{K^*} = \langle \sigma_{K^*\rho \to K\pi} v_{K^*\rho} \rangle n_\rho + \langle \sigma_{K^*\pi \to K\rho} v_{K^*\pi} \rangle n_\pi + \langle \Gamma_{K^*} \rangle. \tag{8}$$

It is interesting to consider the limiting case where the temperature and light meson densities stay constant in time. In this case γ_{K^*} and γ_K are constant and the system (7) can be solved analytically giving the following result:

$$N_{K^*}(\tau) = \frac{\gamma_K}{\gamma} N^0 + \left(N_{K^*}^0 - \frac{\gamma_K}{\gamma} N^0 \right) e^{-\gamma(\tau - \tau_h)},$$
$$N_K(\tau) = \frac{\gamma_{K^*}}{\gamma} N^0 + \left(N_K^0 - \frac{\gamma_{K^*}}{\gamma} N^0 \right) e^{-\gamma(\tau - \tau_h)}, \tag{9}$$
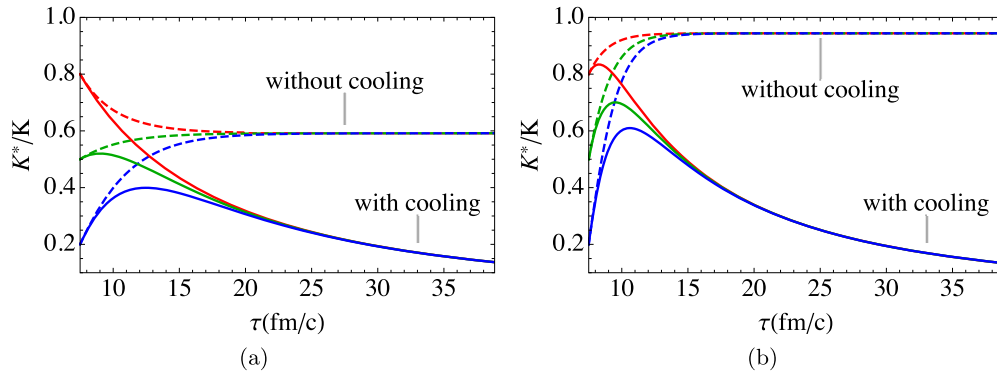
Fig. 3. K^*/K ratio as a function of the proper time τ. Dashed lines correspond to the initial conditions 0.2, 0.5 and 0.8 and no cooling. Solid lines correspond to the initial conditions 0.2, 0.5 and 0.8 and cooling. a) Cross sections from S. H. Lee et al. [16]. b) Cross sections from A. Martinez et al. [17].

where $N^0 = N^0_{K^*} + N^0_K$, i.e., the sum of the initial abundances of K and K^*. Moreover, $\gamma = \gamma_{K^*} + \gamma_K$, as computed in expressions (8). At the hadronization time, τ_h, the system of K^*'s and K's starts to evolve and collide with the light particles from the reservoir which is kept at constant temperature. At large times the $N^0_{K^*}$ and N^0_K reach their asymptotic constant values. This is our operational definition of chemical equilibrium.

Once we define the temperature evolution ("cooling") of the hadron gas $T(\tau)$ and the initial conditions $N_{K^*}(\tau_h)$ and $N_K(\tau_h)$, the system of differential equations (7) can be solved, yielding N_{K^*}, N_K and the ratio $R(\tau)$:

$$R(\tau) = \frac{N_{K^*}}{N_K} = \frac{K^*}{K}. \tag{10}$$

We follow the time evolution of the abundances until the kinetic freeze-out of the gas, which is defined by the freeze-out temperature T_f and occurs at time τ_f. Assuming that the hadronic system undergoes a Bjorken-like expansion, we may write:

$$T = T_h \left(\frac{\tau_h}{\tau}\right)^{1/3}, \tag{11}$$

where $T_h = 175$ MeV is the universal hadronization temperature discussed above and τ_h is the hadronization time, which may change from system to system. We take the above expression at the particular freeze out time, τ_f and freeze-out temperature, T_f, and invert it to obtain:

$$\tau_f = \tau_h \left(\frac{T_h}{T_f}\right)^3. \tag{12}$$

We solve (7) until τ_f and compute the ratio $R[\tau_f(T_f)]$. As it was pointed out long ago [26], the kinetic freeze-out temperature is not an universal constant. It depends on the size of the hadronic system and hence on the collision energy, on the mass number of the colliding nuclei and on the centrality of the collision. A recent blastwave fit analysis made by the ALICE Collaboration [24] has confirmed that the kinetic freeze-out temperature decreases with the system size, customarily associated to the multiplicity density of charged particles, $dN/d\eta$, measured at midrapidity. The empirical relation between T_f and $\mathcal{N}$ found in [24] can be parametrized as:

$$T_f = \frac{T_{f0}}{\mathcal{N}^a}, \tag{13}$$

where T_{f0} and a are constants. Inserting (13) into (12) we find that

$$\tau_f \propto \mathcal{N}^{3a}. \tag{14}$$

This relation tells us that $\mathcal{N}$ gives a measure of the duration of the hadronic phase. Larger systems (with larger $\mathcal{N}$) live longer. Using the obtained τ_f to determine the end of the evolution of (7) we find R as a function $\mathcal{N}$. The function R can then be directly compared with the data on R versus $\mathcal{N}$ presented very recently in [13]. This will be done in the next section.

3. Results and discussion

From what was said above we see that the final multiplicities of K^* and K may depend on: i) the collision dynamics, i.e., on the production and absorption cross sections discussed above; ii) the initial conditions of the evolution equations (7), i.e., the initial values of N_{K^*} and N_K; iii) the expansion dynamics, i.e., the cooling function $T(\tau)$ and iv) the system size, characterized by $dN/d\eta(\eta = 0)$.

We solve the equations (7) using as input the cross sections calculated in [16] and in [17]. The initial temperature is $T_h = 175$ MeV and the initial conditions are $K^*/K = 0.2$, 0.5 and 0.8. The results are shown in Fig. 3. On the left (right) panel the inputs are from Ref. [16] ([17]).

First we observe that, as anticipated from Eqs. (9), when there is no cooling the system evolves to an asymptotic state where the abundances become constant. When cooling (11) is included, the ratio K^*/K drops and at typical freeze-out times of 20 - 25 fm/c reaches 0.2 - 0.3. These numbers are close to the measured ones. This suggests that a cooling faster than (11), such as the Hubble-like cooling discussed in [27,28], is probably incompatible with data. Another interesting aspect of the figure is that, even with cooling, after some
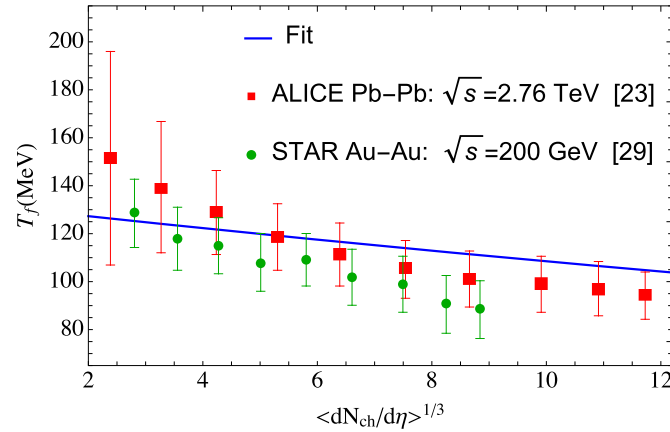
Fig. 4. Freeze-out temperature as a function of $[dN/d\eta(\eta=0)]^{1/3}$. The circles are the result of the blastwave fits of data on Pb + Pb collisions at $\sqrt{s_{NN}}=2.76$ TeV taken by the ALICE Collaboration [24]. The squares represent blastwave fits of data on Au + Au collisions $\sqrt{s_{NN}}=200$ GeV taken by the STAR Collaboration [9]. The line represents the expression (15).

time of evolution the K^*/K ratio becomes the same for all initial conditions. Comparing the left and right panels we observe the effect of changing the microscopic cross sections from those calculated in [16] to those calculated in [17]. When there is no cooling the ratio shown on the left (with the inputs from [16]) is significantly smaller than the one on the right (with the inputs from [17]). This is a consequence of Fig. 2: at higher temperatures, with [17] the cross section for K^* production is bigger and so is the ratio R. It is also for this reason that on the right panel we observe a growth, in some cases very pronounced, of all lines at early times.

In [17] all the cross sections are bigger, all the reactions happen faster and hence the system looses sooner the memory of the initial conditions (the three lines become a single line). Interestingly, at very long times in both cases (right and left panels) the ratio goes to the same value.

From Fig. 3 it is clear that the new reactions mechanisms considered in [17] have an impact on the evolution of the abundances of K^* and K mesons in the hadronic medium. They predict a time evolution of the abundances which is considerably different from previously thought: there is an initial increase in the yield ratio which would not exist without taking into account all the possible mechanisms for the processes in (6). Unfortunately, the differences with respect to the previous calculations of Ref. [16] are washed out during the evolution and in the end the improved cross sections lead to a final yield ratio very close to that computed in Ref. [16].

In order to understand this behavior, it is important to notice from Fig. 2 that even though the cross sections for the annihilation of K^* are larger in Ref. [17] than in Ref. [16], those for the creation of K^* are also larger. For example, Fig. 2b clearly shows that in the case of the creation of K^* through $K\pi \to K^*\rho$, the cross sections from Ref. [17] are one order of magnitude larger than those from [16] and, as time passes, i.e., the gas cools down, the difference between them decreases considerably. The opposite goes for the creation of K^* through $K\rho \to K^*\pi$ (Fig. 2a) but the difference between the cross section in Ref. [17] and Ref. [16] in this case is much smaller.

In order to compare our results with data, we will make use of the connection established in [24] between T_f and $\mathcal{N}$. Although the power law fit (13) is very useful because it leads immediately to (14), a somewhat better fit of the points shown in [24] can be obtained with the form:

$$T_f = T_{f0} e^{-b\mathcal{N}}, \tag{15}$$

where $T_{f0} = 132.5$ MeV and $b = 0.02$. The above expression is compared to the data points from [24] in Fig. 4. We emphasize that Eq. (15) is not the result of a global best χ^2 fit. We try to get a better description of the higher energy data points, which will be relevant for the study of the K^*/K ratio measured at the LHC. The STAR points are shown just for comparison. We first choose the system under consideration, fixing $\mathcal{N}$. This determines the freeze-out temperature, T_f, and the endpoint of the evolution, τ_f. Then, we read the ratio K^*/K from Fig. 3. Finally, we plot K^*/K as a function of $\mathcal{N}$ and compare the results with the data compilation published in [13]. The comparison is presented in Fig. 5.

As it can be seen in Fig. 3, the longer the hadronic system lasts, the smaller is the ratio R. Indeed, for each (increasing) value of $\mathcal{N}$ we stop the evolution at an (increasing) value of τ (which is τ_f) and read from Fig. 3 a (decreasing) value of the ratio K^*/K.

There is a strong correlation between Fig. 4 and Fig. 5. A steeper function in the first figure implies a steeper function in the second. In fact $R \simeq T_f$. Interestingly, the data seem to exclude a flat horizontal line in Fig. 4, i.e., a freeze-out temperature which is universal, independent of the system size.

Knowing that the existence of a hadron gas phase leads to a reduction in the ratio $R = K^*/K$, the systematic study of this ratio in different collisions and at different energies will help us in better determining the properties of the hadron gas. In proton-proton collisions, where there is no hadron gas and hence no K^* absorption, R should be maximal. Moving to p-A and A-A collisions we expect to see the formation of a larger and longer-living hadron gas. Also, when we move to larger systems we observe a growth of the multiplicity of produced particles and also of the multiplicity density in the central rapidity region $\mathcal{N} = dN/d\eta(\eta=0)$, which is usually taken as a measure of the size of the system.

In our approach to study the ratio $R = K^*/K$ we made some simplifications. The goal was to determine which ingredients are really crucial to understand the observed behavior. One of the simplifications was to neglect the volume of the system. The colliding systems mentioned in Fig. 5 are different and so are the corresponding hadronic gases, which have different volumes. In our study these differences are partly considered in Eq. (15). Moreover the details of the light flavor composition of these different systems were not taken into account. In each of the systems considered in Fig. 5 the π and ρ finally measured multiplicities are different. In thermal models, this
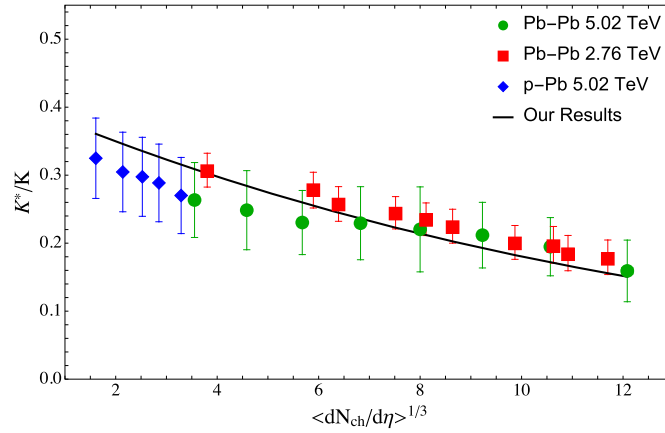
Fig. 5. K^*/K as a function of $[dN/d\eta(\eta=0)]^{1/3}$. Data are from [13].

Table 1
Parameters used in (16). With the above numbers the temperature is given in MeV and the outcome is the thermally averaged cross sections in mb. In the last line, the average decay width is given in fm^{-1}.

	p_0	p_1	p_2	p_3
$K^*\rho \to K\pi$ [17]	92	-0.91	0.0043	-7.2×10^{-6}
$K^*\rho \to K\pi$ [16]	1.78	-0.0052	0.000007	0
$K\pi \to K^*\rho$ [17]	-20	0.6	-0.007	3.5×10^{-5}
$K\pi \to K^*\rho$ [16]	0.2	-0.004	0.00001	6.0×10^{-8}
$K^*\pi \to K\rho$ [17]	-8.5	0.200	-0.00085	1.23×10^{-6}
$K^*\pi \to K\rho$ [16]	-0.1	-0.002	0.00007	-1.5×10^{-7}
$K\rho \to K^*\pi$ [17]	25.3	-0.143	0.00052	-8.0×10^{-7}
$K\rho \to K^*\pi$ [16]	0	0.010	-0.000014	0
$K\pi \to K^*$ [16]	-3	0.27	-0.0019	3.8×10^{-6}
$K^* \to K\pi$ [16]	0.2579	-4.32×10^{-4}	6.0×10^{-7}	-6.5×10^{-10}

difference is usually accounted by the fugacity factor, γ, which should appear multiplying the right side of Eq. (2). We have taken $\gamma = 1$ for π's and ρ's in $p - Pb$ and $Pb - Pb$ collisions. In previous studies with thermal models it was shown that, in $Pb - Pb$ collisions, we could have $\gamma_\pi \simeq 1.3$ and $\gamma_\rho \simeq 1.2$. Changes in these quantities would bring changes in Eqs. (8) and (7). We have checked that, using these values for γ_π and γ_ρ we would obtain, in Fig. 5, curves with the same aspect of the solid line but shifted upwards. For conciseness we decided not to include them in the figure. Furthermore, the used numerical values could be different, such as the hadronization temperature, T_h, or the numbers contained in the parametrizations. None of these changes however would substantially change the curve shown in Fig. 5.

To summarize: we have improved the treatment of the microscopic dynamics of K^*'s. We used all the relevant reaction cross sections involving K^*'s calculated in Ref. [17] as input in the evolution equations (7). We included cooling and the dependence of the freeze-out temperature on the system size. We obtained a very good description of the data published in [13] on $R = K^*/K$ as a function of $dN/d\eta(\eta = 0)$. In order to reproduce the features of Fig. 5 we need the three aspects of the process: i) dominance of the K^* absorption reactions; ii) cooling and iii) system size dependent freeze-out.

4. Appendix

In this appendix we have included the parametrization used to reproduce the thermally averaged cross sections calculated in Ref. [16] and in Ref. [17]. It is given by:

$$\langle \sigma v \rangle (T) = p_0 + p_1 T + p_2 T^2 + p_3 T^3. \tag{16}$$

The coefficients p_i are given in Table 1.

Declaration of competing interest

The authors declare that they have no known competing financial interests or personal relationships that could have appeared to influence the work reported in this paper.

Acknowledgements

References

[1] E. Shuryak, Prog. Part. Nucl. Phys. 62 (2009) 48.

 [2] M. Gyulassy, L. McLerran, Nucl. Phys. A 750 (2005) 30.
 [3] G. Torrieri, J. Rafelski, Phys. Lett. B 509 (2001) 239.
 [4] M. Bleicher, J. Aichelin, Phys. Lett. B 530 (2002) 81.
 [5] J. Rafelski, J. Letessier, G. Torrieri, Phys. Rev. C 64 (2001) 054907.
 [6] A.G. Knospe, C. Markert, K. Werner, J. Steinheimer, M. Bleicher, Phys. Rev. C 93 (2016) 014911.
 [7] J. Steinheimer, J. Aichelin, M. Bleicher, H. Stöcker, Phys. Rev. C 95 (2017) 064902.
 [8] A.G. Knospe, C. Markert, K. Werner, J. Steinheimer, M. Bleicher, arXiv:2102.06797 [nucl-th].
 [9] J. Adams, et al., STAR Collaboration, Phys. Rev. C 71 (2005) 064902.
[10] M.M. Aggarwal, et al., STAR Collaboration, Phys. Rev. C 84 (2011) 034909.
[11] B.B. Abelev, et al., ALICE, Phys. Rev. C 91 (2015) 024609.
[12] J. Adam, et al., ALICE, Phys. Rev. C 95 (2017) 064606.
[13] S. Acharya, et al., ALICE Collaboration, Phys. Lett. B 802 (2020) 135225.
[14] M.E. Bracco, F.S. Navarra, M. Nielsen, Phys. Lett. B 454 (1999) 346.
[15] K.P. Khemchandani, A. Martinez Torres, F.S. Navarra, M. Nielsen, L. Tolos, Phys. Rev. D 91 (2015) 094008.
[16] S. Cho, S.H. Lee, Phys. Rev. C 97 (2018) 034908.
[17] A. Martinez Torres, K.P. Khemchandani, L.M. Abreu, F.S. Navarra, M. Nielsen, Phys. Rev. D 97 (2018) 056001.
[18] Y.S. Oh, T. Song, S.H. Lee, Phys. Rev. C 63 (2001) 034901.
[19] F. Carvalho, F.O. Duraes, F.S. Navarra, M. Nielsen, Phys. Rev. C 72 (2005) 024902.
[20] A. Martinez Torres, K.P. Khemchandani, F.S. Navarra, M. Nielsen, L.M. Abreu, Phys. Rev. D 90 (2014) 114023; 93 (2016), 059902(E).
[21] L.M. Abreu, K.P. Khemchandani, A. Martinez Torres, F.S. Navarra, M. Nielsen, Phys. Lett. B 761 (2016) 303.
[22] L.S. Geng, E. Oset, L. Roca, J.A. Oller, Phys. Rev. D 75 (2007) 014017.
[23] C. Daum, et al., ACCMOR Collaboration, Nucl. Phys. B 187 (1981) 1.
[24] B. Abelev, et al., ALICE Collaboration, Phys. Rev. C 88 (2013) 044910.
[25] G.E. Brown, C.M. Ko, Z.G. Wu, L.H. Xia, Phys. Rev. C 43 (1991) 1881.
[26] Y. Hama, F.S. Navarra, Z. Phys. C 53 (1992) 501.
[27] S.K. Singh, P. Ghosh, J.K. Nayak, arXiv:2007.00053.
[28] P. Ghosh, J.K. Nayak, S.K. Singh, S.K. Agarwalla, Phys. Rev. D 101 (2020) 094004.